Uniport Journal of Engineering and Scientific Research (UJESR)

Vol. 5, Issue 2, 2021, Page 59-75
ISSN: 2616-1192

(www.ujesr.org)

An Overview of Optical Metamaterials and Future Outlook

Obite, F[1], Usman, A.D[2], Jaja, E.T[3], Ijeomah, G[4] and Ikhazuangbe, G.I[5]
[1] Department of Physics, Faculty of Physical Science, Ahmadu Bello University, Zaria Nigeria
[2] Department of Electronic & Telecom. Engin., Ahmadu Bello University, Zaria Nigeria
[3] Department of Electrical & Electronic Engin. Tech., Port Harcourt Polytechnic, Nigeria.
[4] Faculty of Electrical & Electronics Engineering, Universiti Malaysia Pahang, Malaysia.
[5] Department of Electrical/Electronic Engin. Tech., Kenule Saro-Wiwa Polytechnic, Nigeria
*Corresponding author's email: edward.jaja@portharcourtpoly.edu.ng

Abstract
The last two decades have witnessed tremendous research in the field of optical metamaterials. They are artificial materials consisting of sub-wavelength nanoscale structures that permit the development of devices with sharp responses to light, acoustic waves, and heat waves. Metamaterials have unlocked the opportunity of unique and fascinating concepts in optics and photonics applications. This technology is intended to enable novel applications in sensing imaging, quantum information processing, light harvesters, and data storage. In this article, an attempt is made to present the most recent state-of-the-art review in the field of optical metamaterials. Particularly, the recent advances in design, theoretical modeling, and nanofabrication are reviewed with the aim of unifying all other published articles. We reflected on a number of recent progress and technological challenges that ignited new light into metamaterial research and discussed promising future prospects.

Keywords: *Metamaterials, Metasurfaces, Artificial materials, Sub-wavelength structures, Theoretical modeling, Nanofabrication*

Received: 4th January, 2021 *Accepted: 30th March, 2021*

1. Introduction

Man-made metamaterials consisting of sub-wavelength nanoscale structures have recently become an active area of research due to their fascinating novel optical responses, not attainable with natural materials (Hanuka et al., 2018; Hsiao et al., 2017a; Zhao et al., 2014; Yoon et al., 2016; Lheurette, Iwanaga, 2012; Boltasseva and Shalaev, 2008; Smith et al., 2004; Su et al., 2018). Just recently, an extensive study was published on the roadmap of optical metamaterials (Urbas et al., 2016). The unique optical properties, including negative refractive index (Smith et al., 2000; Shelby et al., 2001; Shalaev et al., 2005) and permeability, μ, (Pendry et al., 1999; Linden et al., 2004; Dolling et al., 2005), arise from constructing conventional matter on a sub-wavelength scale where each meta-atom displays an electric or magnetic response which transpires on the wavelength scale actual values of the permeability (and permittivity. The most exciting property of metamaterials is due to their electromagnetic components resulting not merely from their configuration, but equally from their engineered sub-wavelength metallic structures. In the same way, by engineering such man-made materials, we could create materials displaying desired electromagnetic characteristics that are usually not achievable with the available natural materials. The formation of the active magnetic material is perhaps one of the most significant and remarkable applications of metamaterials since all materials, loose their magnetic response naturally, in the region of visible light frequency and thus their μ is constant at unity. The active magnetic metamaterial having $\mu \neq 1$ produces a large number of active novel materials in the region of optical frequency, which permits the manipulation of light freely.

The real industrial commercialization of active metamaterials is yet to be realized, which is attributed to the growing difficulty in constructing matter in three dimensions at the nanoscale. Increasing the operational frequencies of metamaterials, metals, a major constituent of metamaterials become plasmonic (i.e. lossy) as we move towards the optical region. Also, plasmonic materials, such as gold and silver, lack

compatibility with CMOS technology, therefore hindering smooth implementation in current large-scale system fabrication. It is worthy of note that recent research studies explore alternative novel materials with tunable, low-loss, and compatible CMOS metamaterials (West et al., 2010; Naik et al., 2013). Furthermore, all di-electric optical metamaterials at such range of wavelength are expected to possess a minimum thickness similar to the wavelength, this limits fundamentally, the density of states concentration and confined light-matter interaction. Using plasmonic materials for instance as constituents could provide exceptional opportunities to improve these interactions, due to strongly localized fields as a result of surface plasmons (Maier et al., 2001; Maier and Atwater, 2005; Zhao et al., 2014; Ozbay, 2006). Metamaterials have applications among others, ranging from optical cloaking (Cai et al., 2007), optical sensors for detecting biological and chemical species (Jakšić, 2010), imaging (Shvets et al., 2007), laser accelerators (Hanuka et al., 2017), and photonics and plasmonics (Lindquist et al., 2012). Metamaterials also demonstrate high potential for military and defense application (Albertoni, 2011; Brizzi et al., 2012; Chaurasiya et al., 2014; Andersson and Åkerlind, 2014; Jones et al., 2013; Kumar et al., 2016; Zaghloul et al., 2010; Wu, 2018).

The reality of homogeneous materials with negative refractive index was first visualized by Veselago in 1968 (Veselago, 1968), the work has become available for research experts in optics, with the accrued knowledge and facts now being used for the design and actualization of novel metamaterials at any practical frequency of interest. In 2011, a group called Capasso introduced the concept branded as 'interface discontinuities', currently known as 'metasurfaces' as uncertainties started to grow concerning the future prospects of metamaterials (Yu et al., 2011). Also, from a technical and practical point of view, their decreased profile makes them easier and attractive to realize compared to metamaterials. That said, it is pertinent to clarify here that metasurfaces are an array of two-dimensional (2D) meta-atoms having sub-wavelength periodicity, thus, may be considered as a planar analog of active metamaterials having a thickness smaller than the operational wavelength. Excitingly, a significant volume of experimentally achieved metamaterials preceding 2011 is all planar (Linden et al., 2004; Dolling et al., 2005; Shalaev et al., 2005; Henzie et al., 2007; Decker et al., 2007) as a result of fabrication limitations in realizing the three dimensions. The theoretical difference between planar metasurfaces and metamaterials, however, is that the former is characterized by induced magnetic and electric surface currents while the latter is by bulk effective parameters. A system of one dimensional (1D) was deliberated by Capasso's group (Yu et al., 2011). Nevertheless, the study in (Yu et al., 2011) has equally received serious comments because of lack of clear novelty. The work was criticized in twofold; firstly, it is normal to affirm that the clear response of phase-gradient active metasurfaces follow directly the familiar Fraunhofer diffraction (Larouche and Smith, 2012). For instance, the first glance unusual performance of light in active metasurfaces using constant $\pm 2\pi/\Lambda$ phase gradient is equal to the blazed gratings function with period Λ, the main difference is that for blazed gratings the varying linear phase is attained by a sawtooth-shaped, triangular profile. The microwave community gave the second reason for criticizing the work, essentially asserting that phase-gradient active metasurfaces are simply to scale frequency selective surfaces into larger frequencies (Bansal, 2011). Since frequency selective surfaces, as well as the derived theories of reflection and transmission arrays, are made of metal patches of sub-wavelength arrays or apertures inside a metal film which function conventionally as filters (Mittra et al., 1988), flat lenses (McGrath, 1986; Pozar, 1996; Al-Joumayly and Behdad, 2011), and flat parabolic reflectors (Kelkar, 1991; Pozar and Metzler, 1993; Pozar et al., 1997), respectively, hence, metasurfaces and frequency selection may be referred to as two sides of a coin. At this point, it is clearly evident that the maneuvering of electromagnetic waves with flat and thin sub-wavelength devices has remained an ongoing research effort for several years, but recently it's attracting a substantial improvement in virtually every spectrum of the electromagnetic field.

The active research community in optical metamaterials has published a large number of up-to-date reviews and recent advances in the field of optical metamaterials and metasurfaces (Fontana and Ratna, 2015; Fruhnert et al., 2014; Yu and Capasso, 2014; Fleury and Alu, 2014; Ross et al., 2014; Pendry, 2014; Soukoulis and Wegener, 2011; Schuller et al., 2010; Turpin et al., 2014; Lapine et al., 2014; Zheludev and Kivshar, 2012; Kildishev et al., 2013; Meinzer et al., 2014; Estakhri and Alù, 2016; Genevet and Capasso, 2015; Minovich et al., 2015; Walia et al., 2015; Chen et al., 2016; Glybovski et al., 2016; Shaltout et al., 2016; Zhang et al., 2016; Hsiao et al., 2017b; Khorasaninejad et

al., 2017; Lalanne and Chavel, 2017; Zhu et al., 2017). Such accrued knowledge deserves detailed examination in order to define the state-of-the-art and future trends in the field. In this article, an attempt is made to present the most recent state-of-the-art review in the field of optical metamaterials. Particularly, the recent advances in design, theoretical modeling, and nanofabrication are reviewed with the aim of unifying all other published options in optical metamaterials.

2. Structure of optical metamaterials

This section presents the metamaterial technique used in modifying the attractive magnetic permeability of metamaterials in the region of visible frequency and also clarify the appropriate material structures for active metamaterials in the visible region that work as magnetic metamaterials (Ishikawa et al., 2005; Ishikawa and Tanaka, 2006; Ishikawa et al., 2007).

2.1 Optical properties of metals

For metals, in order to explain the dispersion properties in THz to the region of visible light, the internal impedance ($Z_s(\omega)$) for a given unit length with a unit width for a plane conductor is given by:

$$Z_s(\omega) = \frac{1}{\sigma(\omega)\int_0^T \frac{exp[ik(\omega)z + exp[ik(\omega)(T-z)]}{1+exp[ik(\omega)T]}} = R_s(\omega) + iX_s(\omega) \quad (1)$$

$$k(\omega) = \sqrt[\omega]{\varepsilon_0\mu_0\left[1 + i\frac{\sigma(\omega)}{\omega\varepsilon_0}\right]} \quad (2)$$

where $Z_s(\omega)$ consisting of both the real and the imaginary parts are the active surface resistivity R_s and the active internal reactance X_s respectively. Also, from Equation 1, the integral given in the denominator denotes the overall current passing through the whole cross-section of the given conductor.

2.2 Dispersion properties of split-ring resonators

Figure 1 displays the calculated model by means of a split-ring resonator (SRR), proposed by Pendry (Pendry et al., 1999), as the unit element of a metamaterial. As shown in Fig. 1, the ring radius is r, the width of the ring is w, the distance between the two SRR rings is d, the dimension of the unit-cell in the direction of the xy-plane is a, and the distance between the SRRs adjacent planes along the z-axis is l.

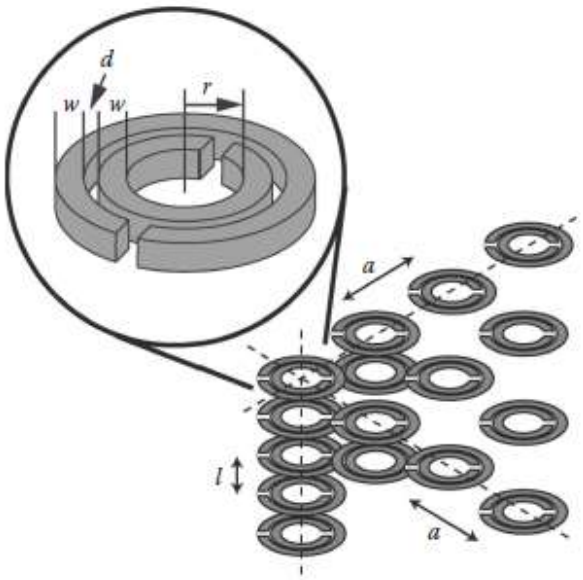

Fig. 1: Outline of the structure of basic optical metamaterials with an SRR used for the artificial control of magnetic permeability (Pendry et al., 1999)

Using the dispersive features of metals defined in Equation 1, and based on their magnetic responses in the optical frequency domain, the frequency dependency was calculated, and μ_{eff} (the effective permeability of the metallic SRRs) is given by Gupta et al' (Chon and Iniewski, 2013) as:

$$\mu_{ff} = \mu_{ff} + i\mu_{ff} = 1 - \frac{F\omega^2}{\omega^2 - 1/CL + i(Z(\omega)\,\omega/L)} \quad (3)$$

where C is geometrical capacitance and L is inductance, F is filling factor and $Z(\omega)$ the metallic ring impedance, defined as (Chon and Iniewski, 2013):

$$F = \frac{\pi r^2}{a^2} \quad (4)$$

$$C = \frac{2\pi r}{3}\varepsilon_0\varepsilon_r\frac{K[(1-t^2)^{1/2}]}{K(t)} \quad (5)$$

$$t = \frac{d}{2w+d} \quad (6)$$

$$L = \frac{\mu_0\pi r^2}{l} \quad (7)$$

$$Z(\omega) = \frac{2\pi r Z_s(\omega)}{w} \quad (8)$$

where K used in Equation (5) is the total elliptic integral of the first-order kind. In order to calculate the geometric capacitance, the formula of Gupta et al. (Garg et al., 2013) was used to evaluate the capacitance flowing per unit length through the distance between the two rings. By means of Equations (1) and (3), the plasma frequency (ω_p) empirical values, and the damping coefficients (γ) of gold, silver, and copper with, ($\omega_p = 13.8 \times 10^{15}\ s^{-1}$ and $\gamma = 107.5 \times 10^{12}\ s^{-1}$for gold, $\omega_p = 14.0 \times 10^{15}\ s^{-1}$ and $\gamma = 32.3 \times 10^{12}\ s^{-1}$ for silver, and $\omega_p = 13.4 \times 10^{15}\ s^{-1}$ and $\gamma = 144.9 \times 10^{12}\ s^{-1}$ for copper), the frequency dispersion μ_{eff} is calculated from 100 to 800 THz (Johnson and Christy, 1972).

At the SRR resonant frequency, μ_{eff} fluctuates both in the positive and negative direction and takes the max μ_{eff} and the min μ_{eff} as shown in Fig. 2, accordingly. The difference in μ_{eff} is described as the change between the max μ_{eff} and the min μ_{eff}, and the calculated results were plotted in Fig. 3, for every metal SRRs. It was clarified from the results that a 3D array of metallic SRRs composed of silver can yield a solid magnetic response in the region of visible light frequency. As shown in Fig. 3, silver SRRs display changes in μ_{eff} beyond 2.0 in the whole visible region, which explains that μ_{eff} can turn out to be a negative value, while the responses of copper and gold SRRs in the region of visible light are less than 2.0.

In Fig. 4, the design approach of optical metamaterials revealing the active magnetic response is shown. In low-frequency region (<100 THz), to achieve a reasonably lower-resonant frequency with lower metal structure resistance, the structure must have both a high geometrical capacitance as well as a wide ring width, and the SRR original shape is appropriate, which is a concentric dual ring with gaps. In contrast, at higher frequency region (>100 THz), the reactance ($X_s(\omega)$) influence becomes more dominant in the ring than the resistance inside the SRR ring. To increase the frequency at resonance, in that higher frequency state, a smaller geometrical capacitance is required by the resonant structure, also, to maintain a high Q-value (quality-value) and adequate SRRs magnetic responses, a larger geometrical inductance is required of the structure.

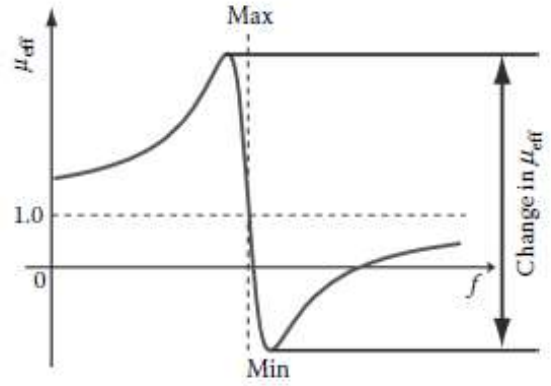

Fig. 2: μ_{eff} changes in the positive and negative direction and takes the max μ_{eff} and the min μ_{eff} at the SRR resonant frequency (Chon and Iniewski, 2013)

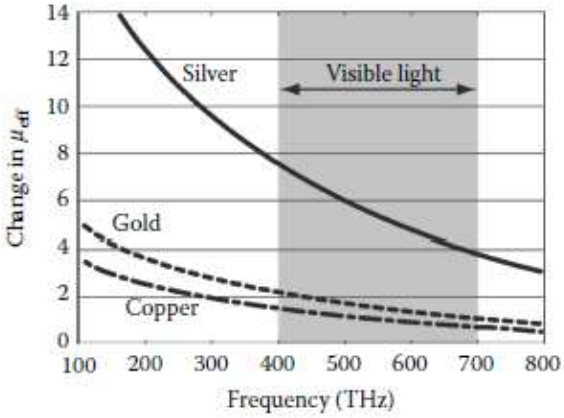

Fig. 3: The frequency dependence of change in μ_{eff} of the SRRs consisting of silver, gold, and copper (Chon and Iniewski, 2013)

Fig. 4: The design approach of optical metamaterials in the optical frequency region revealing the active magnetic response below and above 100 THz (Chon and Iniewski, 2013)

3. Theoretical modeling (electromagnetic homogenization of optical metasurfaces)

Homogenization is the process of introducing effective material parameters in media composed of particles (Simovski, 2010). Essentially, two main methods are used for assessing the electromagnetic responses of active metamaterial surfaces: the first method employs the retrieval technique using scattering features arising from the distinct metasurface; the second method is based on the concept of homogenization, which evaluates the metal lattice structures and their constituent electromagnetics. The first method is similar to the technique employed for 3D metamaterial modeling. For 3D structures, there is a finite thickness that matches the size of the sample; for 2D optical metasurfaces, a negligible thickness is typically assumed, meaning that, the homogenized array is a uniform sheet, thus the transmission and reflection are interpreted in terms of an induced average surface currents (Holloway et al., 2011). Homogenization, in contrast, deals with the average surface constitutive factors that describe the average microscopic structures constituting the metasurfaces. Homogenization takes cognizance of the field interactions inside the array and considers the microscopic induced currents. Using the electric and magnetic sheet currents, the homogenized parameters can be defined for instance, the surface vulnerabilities, to relay the fields and that of the induced metasurface currents.

Several preceding studies have deliberated the complete homogenization of optical metasurfaces consisting of simple inclusions, for example, inclusions such as spheres or planar (Holloway et al., 2005; Holloway et al., 2012; Dimitriadis et al., 2012b; Albooyeh et al., 2011; Morits and Simovski, 2010; Holloway et al., 2009; Dimitriadis et al., 2012a; Mousavi et al., 2012). Generally, for arbitrary metasurfaces, the surface susceptibility is a 6-by-6 tensor, while the currently existing models are formulated using 3-by-3 tensor (Dimitriadis et al., 2012b) or in scalar (Holloway et al., 2005) because of specific assumptions on the impinging field and the symmetry of the inclusions. Therefore, a general model for arbitrary optical metasurfaces is currently not available. A complete model would take into consideration all possible electric and magnetic coupling effects. To this end, some authors considered a periodic material surface and developed a 2D generalized homogenization standard model. They further extended the models presented by earlier studies (Holloway et al., 2005; Holloway et al., 2012; Dimitriadis et al., 2012b; Holloway et al., 2009) to develop a generalized and effective standard based on a 6-by-6 tensor. The developed model is presented in the following subsection.

3.1 Surface susceptibility

Consider a periodic infinite 2D array as shown in Fig. 5, consisting of unit sub-wavelength cells having a period d filled with arbitrary inclusions (Zhao et al., 2014).

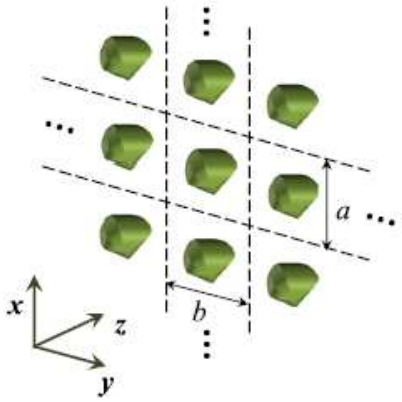

Fig. 5: A periodic infinite 2D metasurface (Zhao et al., 2014)

For a unit isolated cell, p_0 is induced electric dipole and m_0 is induced magnetic dipole, which can be stated by:

$$\begin{Bmatrix}\mathbf{p}_0\\ \mathbf{m}_0\end{Bmatrix} = \alpha \begin{Bmatrix}\mathbf{E}^{\mathrm{loc}}\\ \mathbf{H}^{\mathrm{loc}}\end{Bmatrix} = \begin{bmatrix}\boldsymbol{\alpha}^{\mathrm{ee}} & \boldsymbol{\alpha}^{\mathrm{em}}\\ \boldsymbol{\alpha}^{\mathrm{me}} & \boldsymbol{\alpha}^{\mathrm{mm}}\end{bmatrix} \begin{Bmatrix}\mathbf{E}^{\mathrm{loc}}\\ \mathbf{H}^{\mathrm{loc}}\end{Bmatrix} \tag{9}$$

where α is generally an array element of 6-by-6 tensor, while E^{loc} and H^{loc} are the calculated local fields. By considering the 2D array induced dipoles, the local fields can be stated as:

$$\begin{Bmatrix}\mathbf{E}^{\mathrm{loc}}\\ \mathbf{H}^{\mathrm{loc}}\end{Bmatrix} = \begin{Bmatrix}\mathbf{E}^{\mathrm{inc}}\\ \mathbf{H}^{\mathrm{inc}}\end{Bmatrix} + \begin{Bmatrix}\mathbf{E}^{\mathrm{Array}}\\ \mathbf{H}^{\mathrm{Array}}\end{Bmatrix} \tag{10}$$

where

$$\begin{Bmatrix}\boldsymbol{E}^{Array}\\ \boldsymbol{H}^{Array}\end{Bmatrix} = \mathbf{C}^{2\mathrm{D}} \begin{Bmatrix}\mathbf{p}_0\\ \mathbf{m}_0\end{Bmatrix} \tag{11}$$

denote the scattering coming from adjacent unit cells which could be determined using Green's dyads C^{2D} that is built on the theorem of Bloch (Dimitriadis et al., 2012b; Morits and Simovski, 2010; Dimitriadis et al., 2012a; Mousavi et al., 2012; Beruete et al., 2006; Sounas and Kantartzis, 2009; Belov and Simovski, 2005) for a specified transverse wave amount moving on the array. Putting Equations (10) and (11) into (9) offers the

relationship connecting the dipole moments with the incident fields:

$$\begin{Bmatrix}\mathbf{p}^0\\ \mathbf{m}^0\end{Bmatrix} = (\boldsymbol{\alpha}^{-1} - \mathbf{C}^{2\mathrm{D}})^{-1}\begin{Bmatrix}\mathbf{E}^{\mathrm{inc}}\\ \mathbf{H}^{\mathrm{inc}}\end{Bmatrix} \quad (12)$$

The metasurface can then be modeled as a sheet with uniform average surface susceptibility (Kuester et al., 2003), defined as:

$$\begin{Bmatrix}\mathbf{P}\\ \mathbf{M}\end{Bmatrix} = x^{2\mathrm{D}}\begin{Bmatrix}\mathbf{E}^{\mathrm{surf}}\\ \mathbf{H}^{\mathrm{surf}}\end{Bmatrix} = x^{2D}\left(\begin{Bmatrix}\mathbf{E}^{\mathrm{inc}}\\ \mathbf{H}^{\mathrm{inc}}\end{Bmatrix} + \begin{Bmatrix}\mathbf{E}^{\mathrm{scat}}\\ \mathbf{H}^{\mathrm{scat}}\end{Bmatrix}\right) \quad (13)$$

whereby the average polarizations are expressed as $\mathrm{P} = \mathrm{p}_0/ab$ and $\mathrm{M} = \mathrm{m}_0/ab$, while the fields $\mathrm{E}^{\mathrm{surf}}$and $\mathrm{H}^{\mathrm{surf}}$ are introduced by the fields of incidence ($\mathrm{E}^{\mathrm{inc}}$ and $\mathrm{H}^{\mathrm{inc}}$) and also scattered fields ($\mathrm{E}^{\mathrm{scat}}$ and $\mathrm{H}^{\mathrm{scat}}$) produced in the array by all the induced dipoles.

From Fig. 6(a), the authors in (Zhao et al., 2014) show the fields on each side of the surface array plane produced by an active electric current element J_{sx}, which creates the opposite transverse active magnetic fields ($\mathrm{H}^{0-} = -\mathrm{H}^{0+}$) through the plane, which also generates transmitting electric fields ($\mathrm{E}^{0+} = \mathrm{E}^{0-}$) on each sides of the surface through the x-direction.

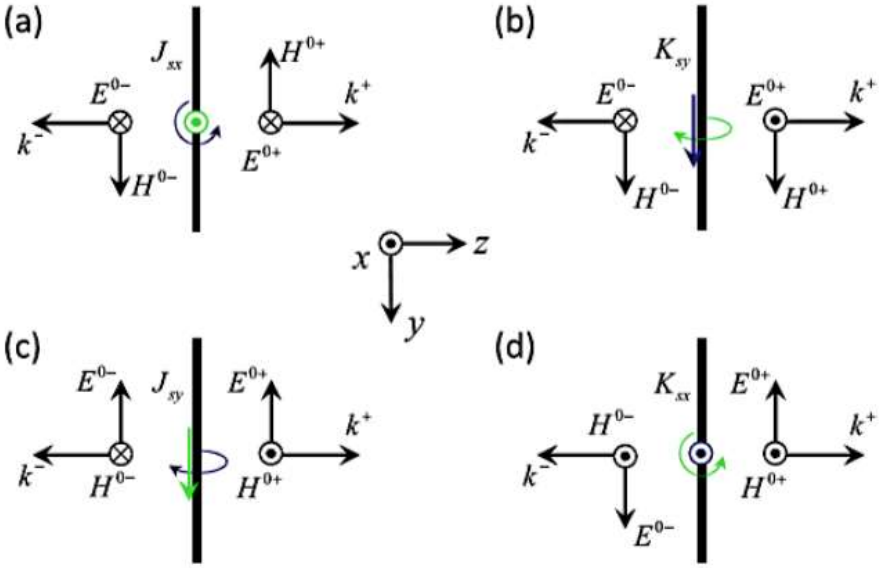

Fig. 6: Surface-induced currents and the radiated associated fields on the metasurface (Zhao et al., 2014)

The active electric currents are connected to the cutoff magnetic fields through the surface (Zhao et al., 2014):

$$\hat{\mathrm{z}} \times (\mathbf{H}^{0+} - \mathbf{H}^{0-}) = \hat{\mathrm{z}} \times (2\mathrm{H}^{0+})\hat{\mathrm{y}} = -2\mathrm{H}^{0+}\hat{\mathrm{x}} = J_{sx}\hat{\mathrm{x}}$$

$$\hat{\mathrm{z}} \times (\mathbf{H}^{0+} - \mathbf{H}^{0-}) = \hat{\mathrm{z}} \times (-2\mathrm{H}^{0-})\hat{\mathrm{y}} = 2\mathrm{H}^{0-}\hat{\mathrm{x}} = J_{sx}\hat{\mathrm{x}} \quad (14)$$

Thus, $\mathrm{H}^{0+} = -J_{sx}/2$ and $\mathrm{H}^{0-} = J_{sx}/2$, respectively. Furthermore, the electric field and magnetic field can be related through the impedance of the wave (Pozar):

$$\mathrm{Z}_0^{\mathrm{TE}} = \frac{E_x}{H_y} = \frac{-E_y}{H_x} = \frac{\omega\mu_0}{k_z} = \frac{k_0\eta_0}{k_z}$$

$$\mathrm{Z}_0^{\mathrm{TE}} = \frac{E_x}{H_y} = \frac{-E_y}{H_x} = \frac{k_z}{\omega\varepsilon_0} = \frac{k_z\eta_0}{k_0} \quad (15)$$

The scattered fields average on the surface are:

$$E_x^{\mathrm{scat}-J_{sx}} = \frac{E_x^{0+} + E_x^{0-}}{2} = \frac{Z_0^{TE}}{2}J_{sx}$$

$$H_y^{\mathrm{scat-k_{sy}}} = \frac{H_y^{0+} + H_y^{0-}}{2} = -\frac{1}{2Z_0^{TE}}K_{sy} \quad (16)$$

$$E_y^{\mathrm{scat-J_{sy}}} = \frac{E_y^{0+} + E_y^{0-}}{2} = \frac{\mathrm{Z}_0^{\mathrm{TM}}}{2}J_{sy}$$

$$H_x^{\mathrm{scat-J_{sy}}} = \frac{H_y^{0+} + H_y^{0-}}{2} = 0 \quad (17)$$

And

$$E_y^{\mathrm{scat-k_{sx}}} = \frac{E_y^{0+} + E_y^{0-}}{2} = 0$$

$$H_x^{\mathrm{scat-k_{sx}}} = \frac{H_y^{0+} + H_y^{0-}}{2} = -\frac{1}{2\mathrm{Z}_0^{\mathrm{TM}}}K_{sx} \quad (18)$$

By taking Equations (16) to (19) in addition to the relationship between the induced dipole moments and the currents (Idemen, 1988):

$$\mathbf{J} = j\omega\mathbf{P}_{\parallel} - \frac{1}{\mu_0}\hat{\mathbf{z}} \times \nabla M_{\perp}$$
$$\mathbf{K} = j\omega\mathbf{M}_{\parallel} + \frac{\mathbf{1}}{\boldsymbol{\varepsilon_0}}\hat{\mathbf{z}} \times \nabla P_{\perp} \quad (19)$$

The scattered fields can be expressed in the form of average surface polarization (Zhao et al., 2014), resulting in:

$$\begin{Bmatrix}\mathbf{E}^{\text{scat}}\\ \mathbf{H}^{\text{scat}}\end{Bmatrix} = \mathbf{Q}\begin{Bmatrix}\mathbf{P}\\ \mathbf{M}\end{Bmatrix} \quad (20)$$

where Q denotes:

$$\begin{Bmatrix} \frac{jk_0^2}{2k_z\varepsilon_0} & 0 & 0 & 0 & 0 & \frac{jk_yk_0c}{2k_z} \\ 0 & \frac{-jk_z}{2\varepsilon_0} & 0 & 0 & 0 & 0 \\ 0 & 0 & \frac{jk_y^2}{2k_z\varepsilon_0} & \frac{jk_yk_0c}{2k_z} & 0 & 0 \\ 0 & 0 & \frac{jk_yk_0c}{2k_z} & \frac{jk_0^2}{2k_z\mu_0} & 0 & 0 \\ 0 & 0 & 0 & 0 & \frac{jk_z}{2\mu_0} & 0 \\ \frac{jk_0k_yc}{2k_z} & 0 & 0 & 0 & 0 & \frac{jk_y^2}{2k_z\mu_0} \end{Bmatrix} \quad (21)$$

Hence, Equation (5) can be rewritten as:

$$\begin{Bmatrix}\mathbf{P}\\ \mathbf{M}\end{Bmatrix} = x^{2\text{D}}\begin{Bmatrix}\mathbf{E}^{\text{surf}}\\ \mathbf{H}^{\text{surf}}\end{Bmatrix} = (ab(\boldsymbol{\alpha}^{-1} - \mathbf{C}^{2\text{D}}) + \boldsymbol{Q})\begin{Bmatrix}\boldsymbol{P}\\ \boldsymbol{M}\end{Bmatrix} \quad (22)$$

Also, the susceptibility homogenized surface y is written as:

$$x^{2\text{D}} = \left(ab\left(\boldsymbol{\alpha}^{-1} - \mathbf{C}^{2\text{D}}\right) + \boldsymbol{Q}\right)^{-1} \quad (23)$$

For a more simplified scenario of uniaxial anisotropic inclusions, a related equation was derived in (Dimitriadis et al., 2012b) under the incidence of TE-wave. In the case of uniaxial, an assumption is made that the inclusions lie only on the metasurface plane. In this universal model, the arbitrary non-contact sub-wavelength inclusions may be modeled and description of the total field coupling array, as presented in the following (Zhao et al., 2014).

$$\begin{Bmatrix}\mathbf{P}\\ \mathbf{M}\end{Bmatrix} = x^{2\text{D}}\begin{Bmatrix}\mathbf{E}^{\text{surf}}\\ \mathbf{H}^{\text{surf}}\end{Bmatrix} = \frac{1}{2}x^{2\text{D}}\left(\begin{Bmatrix}\mathbf{E}^{\text{inc}}\\ \mathbf{H}^{\text{inc}}\end{Bmatrix}\Big|_{\text{z=0}} + \begin{Bmatrix}\mathbf{E}^{\text{refl}}\\ \mathbf{H}^{\text{refl}}\end{Bmatrix}\Big|_{\text{z=0}} + \begin{Bmatrix}\mathbf{E}^{\text{tran}}\\ \mathbf{H}^{\text{tran}}\end{Bmatrix}\Big|_{\text{z=0+}}\right) \quad (24)$$

The incident plane waves may be separated into its corresponding TE mode and TM mode, having transverse electric and magnetic fields (Zhao et al., 2014):

$$\mathbf{E}_{\text{TE}}^{\text{inc}} = E_{\text{TEO}}e^{-j(k_ww+k_zz)}[1\ 0\ 0\ ]^T$$
$$\mathbf{H}_{\text{TE}}^{\text{inc}} = \frac{E_{TEO}e^{-j(k_ww+k_zz)}}{\eta_0}[0\ \ cos\theta\ \ -sin\ \theta]^T \quad (25)$$

$$\mathbf{E}_{\text{TE,TE}}^{\text{refl}} = E_{\text{TEO}}R_{TE,TE}e^{-j(k_ww+k_zz)}[1\ 0\ 0\ ]^T$$
$$\mathbf{H}_{\text{TE,TE}}^{\text{refl}} = \frac{E_{TEO}R_{TE,TE}}{\eta_0}e^{-j(k_ww+k_zz)} \times [0\ \ -cos\theta\ \ -sin\ \theta]^T \quad (26)$$

$$\mathbf{E}_{\text{TE,TE}}^{\text{tran}} = E_{\text{TEO}}T_{TE,TE}e^{-j(k_ww+k_zz)}[1\ 0\ 0\ ]^T$$
$$\mathbf{H}_{\text{TE,TE}}^{\text{tran}} = \frac{E_{TEO}T_{TE,TE}}{\eta_0}e^{-j(k_ww+k_zz)} \times [0\ \ cos\theta\ \ -sin\ \theta]^T \quad (27)$$

$$\mathbf{E}_{\text{TM,TE}}^{\text{refl}} = \frac{E_{TEO}R_{TM,TE}}{\eta_0}e^{-j(k_ww+k_zz)}[0\ \ cos\theta\ \ sin\ \theta]^T$$
$$\mathbf{H}_{\text{TM,TE}}^{\text{refl}} = E_{TEO}R_{TM,TE}e^{-j(k_ww+k_zz)}[1\ 0\ 0\ ]^T \quad (28)$$

$$\mathbf{E}_{\text{TM,TE}}^{\text{tran}} = \frac{E_{TEO}T_{TM,TE}}{\eta_0}e^{-j(k_ww+k_zz)}[0\ \ cos\theta\ \ -sin\ \theta]^T$$
$$\mathbf{E}_{\text{TM,TE}}^{\text{tran}} = E_{TEO}T_{TM,TE}e^{-j(k_ww+k_zz)}[1\ 0\ 0\ ]^T \quad (29)$$

where E_{TEO} represents the field amplitude, TM' subscripts signify TE and TM fields produced by the incident TE waves. The authors in (Zhao et al., 2014) adopted a related coordinate system of vwz, defined alongside the transverse electric field constituent in TE mode as depicted in Fig. 7. For the complete case of TE mode displayed in (a) and (b), the effective transverse field element E^{TH} is resting on the xy-direction towards v- axis. Also,

from (c) and (d) the element H^{TM} of the complete TM mode is resting on the xy-plane and fixed along the v-axis.

The main motive for adopting the fresh coordinate system was to streamline the electromagnetic field's expression in the equations above. The field components can be transformed from the coordinate of the xyz system to vwz system through the transformation matrix (Zhao et al., 2014):

$$\mathbf{T} = \begin{Bmatrix} \cos\theta & \sin\theta & & & \\ -\sin\theta & \cos\theta & & 0 & \\ & & 1 & & \\ & & & \cos\theta & \sin\phi \\ & 0 & & -\sin\theta & \cos\theta \\ & & & & & 1 \end{Bmatrix} \quad (30)$$

Also, for TM polarization, the incident reflected and transmitted fields are (Zhao et al., 2014):

$$\mathbf{H}_{\mathrm{TM}}^{\mathrm{inc}} = H_{\mathrm{TMO}} e^{-j(k_w w + k_z z)} [1\ 0\ 0\ ]^T$$

$$\mathbf{E}_{\mathrm{TM}}^{\mathrm{inc}} = \frac{H_{TMO} e^{-j(k_w w + k_z z)}}{\eta_0} [0 \quad -cos\theta \quad sin\,\theta]^T \quad (31)$$

$$\mathbf{H}_{\mathrm{TM,TM}}^{\mathrm{refl}} = H_{TMO} R_{TM,TM} e^{-j(k_w w - k_z z)} [1\ 0\ 0\ ]^T$$

$$\mathbf{E}_{\mathrm{TM,TM}}^{\mathrm{refl}} = \frac{H_{TMO} R_{TM,TM}}{\eta_0} e^{-j(k_w w - k_z z)} [0 \ \ cos\theta \ \ sin\,\theta]^T \quad (32)$$

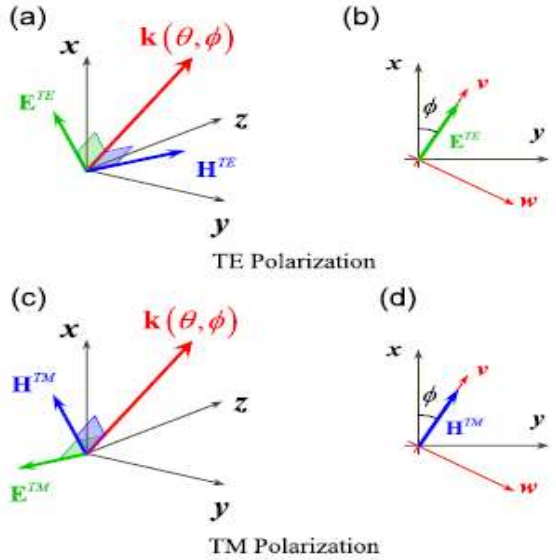

Fig. 7: The complete TE and TM modes (Zhao et al., 2014).

$$\mathbf{H}_{\mathrm{TM,TM}}^{\mathrm{tran}} = H_{\mathrm{TMO}} T_{TM,TM} e^{-j(k_w w + k_z z)} [1\ 0\ 0\ ]^T$$

$$\mathbf{E}_{\mathrm{TM,TM}}^{\mathrm{tran}} = \frac{H_{TMO} T_{TM,TM}}{\eta_0} e^{-j(k_w w + k_z z)} [0 \quad -cos\theta \quad sin\,\theta]^T \quad (33)$$

$$\mathbf{H}_{\mathrm{TE,TM}}^{\mathrm{refl}} = \frac{H_{TMO} R_{TE,TM}}{\eta_0} e^{-j(k_w w - k_z z)} \times [0 \quad -cos\theta \ - \ sin\,\theta]^T$$

$$\mathbf{E}_{\mathrm{TE,TM}}^{\mathrm{refl}} = H_{\mathrm{TMO}} R_{TE,TM} e^{-j(k_w w - k_z z)} [1\ 0\ 0\ ]^T \quad (34)$$

$$\mathbf{H}_{\mathrm{TE,TM}}^{\mathrm{tran}} = \frac{H_{TMO} T_{TE,TM}}{\eta_0} e^{-j(k_w w + k_z z)} [0 \ \ cos\theta \ -\ sin\,\theta]^T$$

$$\mathbf{E}_{\mathrm{TE,TM}}^{\mathrm{tran}} = H_{\mathrm{TMO}} T_{TE,TM} e^{-j(k_w w + k_z z)} [1\ 0\ 0\ ]^T \quad (35)$$

where H_{TMO} is the intruding magnetic field amplitude. The surface currents can be defined by way of comparing the fields through the surface (Zhao et al., 2014):

$$\mathbf{J}_{\mathrm{S1}} = \hat{\mathbf{z}} \times (\mathbf{H}_{\mathrm{z=0^+}} - \mathbf{H}_{\mathrm{z=0^-}}) = \hat{\mathbf{z}} \times \left[\mathbf{H}^{\mathrm{tran}} - \left(\mathbf{H}^{\mathrm{inc}} + \mathbf{H}^{\mathrm{refl}}\right)\right]$$

$$\mathbf{K}_{\mathrm{S1}} = -\hat{\mathbf{z}} \times (\mathbf{E}_{\mathrm{z=0^+}} - \mathbf{E}_{\mathrm{z=0^-}}) = -\hat{\mathbf{z}} \times \left[\mathbf{E}^{\mathrm{tran}} - \left(\mathbf{E}^{\mathrm{inc}} + \mathbf{E}^{\mathrm{refl}}\right)\right] \quad (36)$$

By using Equations (20) and (25), the surface currents $(\mathrm{J_{S2}}, \mathrm{K_{S2}})$ may also be obtained using the plane average fields. Hence, by considering the overall polarization of TE and TM, in which case the directions are alternated by ϕ with reference to x-axis, as displayed in Figures 7(b) and (d), the Q tensor needs to be rotated in the definition of susceptibility (Zhao et al., 2014):

$$x^{2\mathrm{D}} = \left(ab\left(\boldsymbol{\alpha}^{-1} - \mathbf{C}^{2\mathrm{D}}\right) + \boldsymbol{T}^{-1}\boldsymbol{Q}\boldsymbol{T}\right)^{-1} \quad (37)$$

In the case of TE excitation, the surface currents may be forced to satisfy both limitations, resulting in the following set of simultaneous equations (Zhao et al., 2014),

$$\mathbf{J}_{\mathrm{S1}} = \mathbf{J}_{\mathrm{S2}}$$

$$\mathbf{K}_{\mathrm{S1}} = \mathbf{K}_{\mathrm{S2}} \quad (38)$$

where there exist four unknown factors for the active transmission and active reflection coefficients $R_{TE,TE}$, $T_{TE,TE}$, $R_{TM,TE}$, and $T_{TM,TE}$

In summary, for a given metasurface consisting of random inclusions, it has been shown that the transmission and reflection coefficients of random TE and TM waves can be analytically related to the metasurface susceptibility tensor (Zhao et al., 2014).

4. Nanofabrication of optical metamaterials

The artificial optical metamaterials consist of structural units of patterns that are made up of several single nanoscale active building blocks using realistically designed arrangements and geometries. The basic foundation for metamaterials is nano-structured engineering, with significant limitations to their industrial realization. So far, their fabrication is mostly through top-down methods, for instance, interference lithography. The top-down approaches give excellent special control and localization of structures. Nevertheless, they are limited in two-dimensional morphology, and control of structural configuration which hinders their practical implementation. Such as, the loss of energy due to intrinsic material constraint has greatly delayed the device fabrication (Khurgin, 2015). The nano-fabrication of only 2D nanostructures on active planar substrates has been possible thus far because conventional fabrication techniques were not possible in realizing 3D nano-structures. Usually, they were precisely thin hence the term "metasurfaces". Even though metasurfaces have displayed several exotic physical characteristics and uses, they possess critical impediments such as inhomogeneous and also anisotropic optical features of narrow bandwidth, and angle of incidence and polarization dependence (Rho, 2017).

Consequently, to overcome these impediments for optimal performance, it has become paramount to identify novel materials, 3D nano-fabrication techniques must be developed. Thus, colloidal nano-particles (NPs) offer remarkable performance properties, such as excellent structural control, crystallinity, minimized loss, tunable optical response with broadband behaviour.

Though the utilization of self-assembly methods for the fabrication of metamaterial is still new, current progress is exposing their prospects. The research models consist of using atomic layer deposition and block copolymer self-assembly to adjust the light concentration features as shown in Fig. 8(a) (Hägglund et al., 2013), with similar repetition in metallic 3D gold (Au) nano-structure for displaying the optical chirality (Fig. 8(b)) (Vignolini et al., 2012) with tunable plasmonic connection (Ye et al., 2013a).

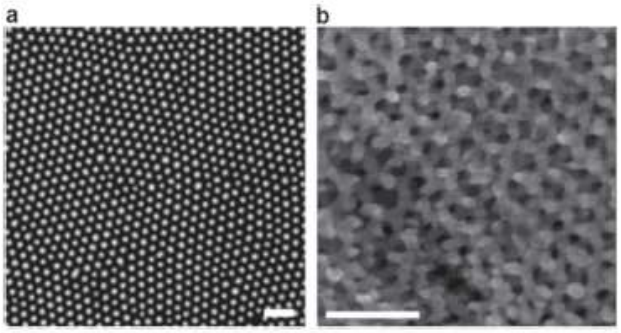

Fig. 8: SEM Images (a) hexagonal structure of Au dot array using thin-film deposition (b) a basic 3D Au network produced by electrodeposition template (Urbas et al., 2016).

4.1 Nano-particles (NPs) for nano-fabrication of optical metamaterials

NPs are man-made building structures employed for developing metamaterials operating in the near-infrared visible region. Progresses in synthetic biochemical approaches permit the organized development of metallic colloidal NPs (Rycenga et al., 2011) as displayed in Fig. 9(a) to 9(c), with heavily doped semiconductors (Ye et al., 2014; Buonsanti and Milliron, 2013) (Fig. 9(d) to 9(f)). Similarly, the NPs can be customized in size and shape (Ye et al., 2013b; Lohse and Murphy, 2013) and configuration to adjust the carrier concentration, dielectric constant, and carrier relaxation and thus the spectral location and the width of plasmonic resonance with the spatial distribution of the resultant electrical fields. The active NPs could be self-assembled or directed (Fan et al., 2012; Ross et al., 2015) towards assembling from a solution as shown in Fig. 9(g) and Fig. 9(h) (Ye et al., 2013a).

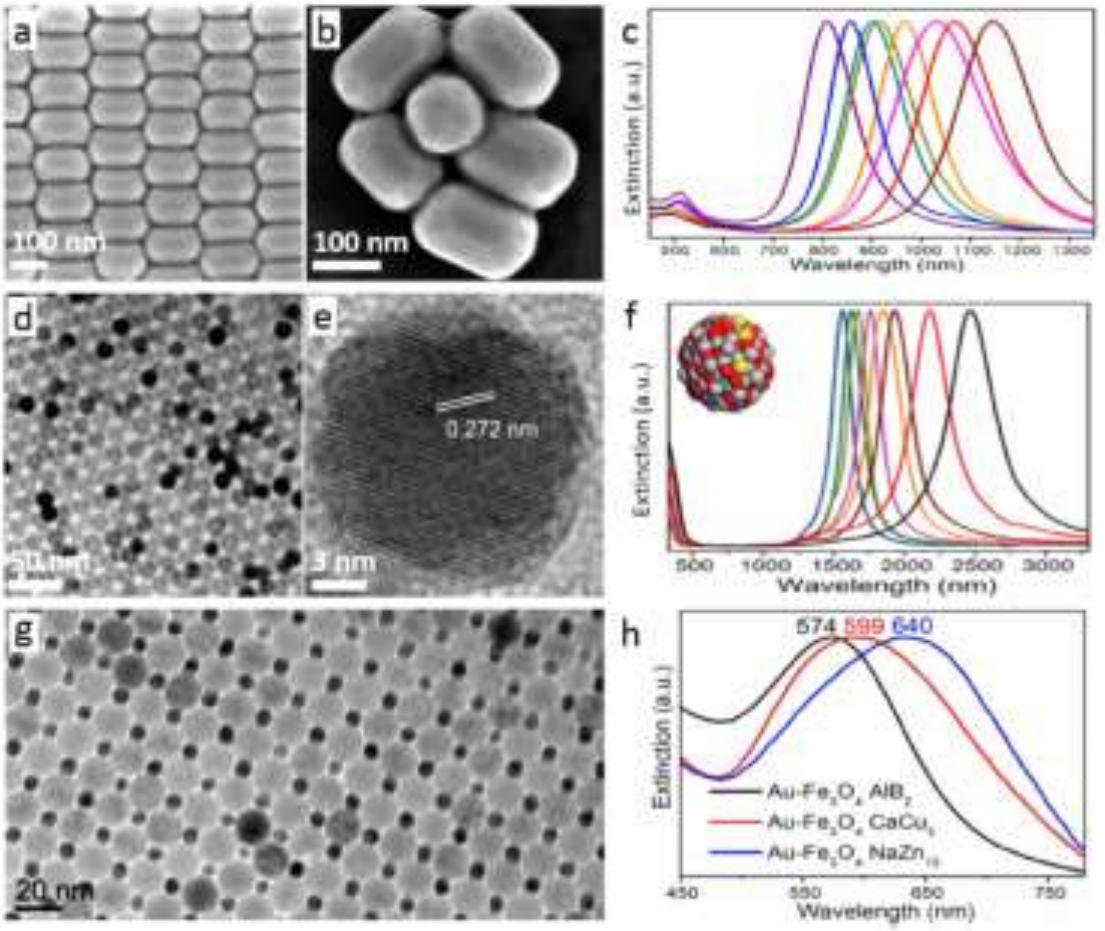

Fig. 9: (a) Low-resolution SEM image (b) high-resolution SEM image (c) the spectra display of Au nanorods. (d) Low-resolution TEM image (e) high-resolution TEM image (f) spectra display of CdO: F, in colloidal NPs. (g) TEM image (h) the spectra of A_u-Fe_3O_4 binary colloidal NP superlattices (Urbas et al., 2016)

The concentration, composition, orientation, and organization of the colloidal NPs within the assembly permit information flow throughout the system. Inter-particle spaces and connections are adjusted by substituting the metal active ligand chemistry while synthesizing (Fig. 10(a)). Similarly, combined communications among adjacent NPs will induce characteristics of the mesoscale (Fig. 10(b) and Fig. 10(c)) (Fafarman et al., 2012). The Manufacturing assemblies as a result of NP interactions permit the design of effective multi-materials with responses not seen in bulk. NPs can be reasonably printed and effectively patterned to create sub-wavelength; colloidal NP-based excellent structures are also called 'meta-atoms'. They are built from NPs and permit the hierarchical design of 2D optical metasurfaces, leveraging on the active excellent features of the colloidal NP. Such as its application in filtering using bandstop tunable as shown in Fig. 10(d) to Fig. 10(f)) (Fafarman et al., 2012), with controlled polarized transmitted light for designing complex structures (Chen et al., 2015). Optical metasurfaces and metamaterials can be fabricated on a vast area by means of solution-based printing methods.

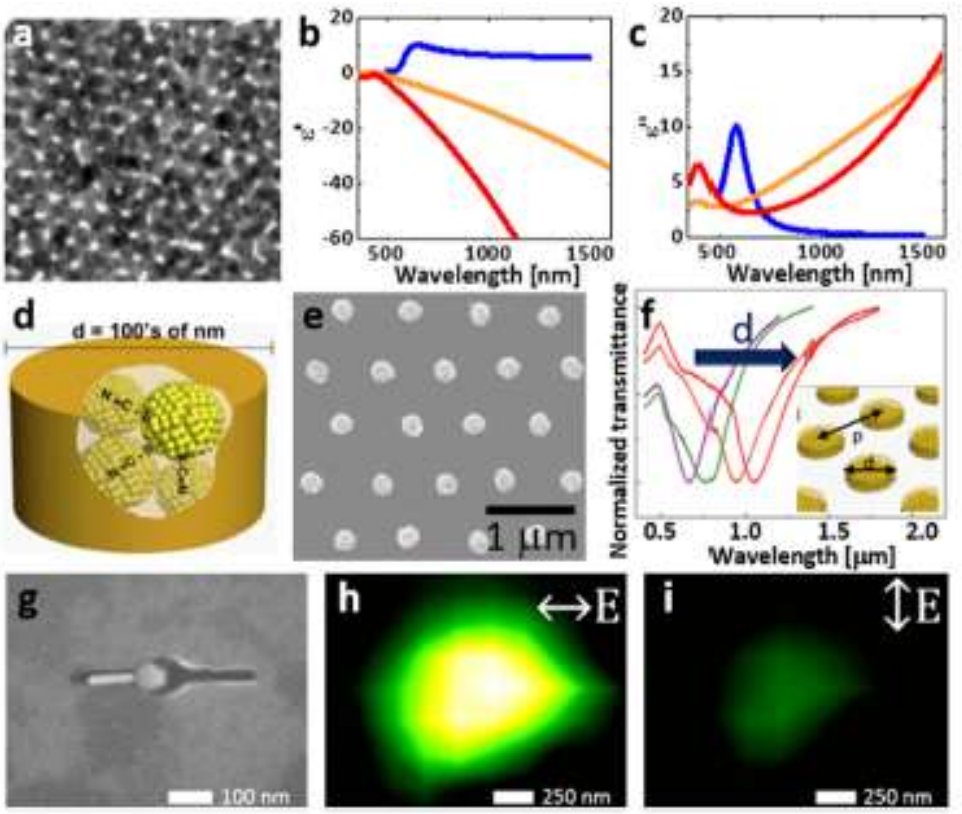

Fig. 10: (a) TEM image of thiocyanate (SCN)-exchanged Au NC film. (b) The real and (c) the imaginary active dielectric functions from oleic acid-capped (blue) and SCN-exchanged (orange) Au NC films with bulk Au (red). (d) The schematic diagram, (e) A SEM image, and (f) the spectral transmittance of nanoimprinted with SCN-exchanged Au NC-based nanopillar arrays ($d = 120$ to $300\ nm$) (g) A SEM image of Au nanorod (h) nano-phosphor heterodimer (i) A polarized-dependent improved radiation (Urbas et al., 2016).

5. Recent progress and technological challenges

Genetic optimized algorithms have recently been effectively applied to plasmonic nano-antennas (Forestiere et al., 2012) as well as negative-index dielectric metamaterials (Dong and Liu, 2012), indicating optimum aperiodic results. Nevertheless, substantial progress is required for the development of advanced simulation software that is able to cope with device complexity, in order to take advantage of their full potentials. Other paths for manufacturing aperiodic metamaterials are digitally obtainable (Urbas et al., 2016), programming design, or coding (Cui et al., 2014). In line with the aforementioned, metastructures can be digitally synthesized to produce excellent performance properties by accurately molding 2-bits materials into functional local units of metamaterial bytes. In contrast to conventional material structures, usually challenged with long-term periodicity, effective digitally synthesized metamaterials (Forestiere et al., 2012) retain precise active structures purely constructed by combining 2-bits nanoscale structures. Consequently, carefully designed spatial local ordering influences the determination of the properties of effective digital metamaterial (Urbas et al., 2016).

The last route to aperiodic metamaterials is employing quasi-crystals and that of aperiodic tilings, also known as ‘geometrical approach’. The method, which is essentially entrenched in geometry has largely been studied in nano-photonics, which results in several device applications such as optical sensing, light sources, non-linear optics, solar cells, and energy harvesting (Forestiere et al., 2012). The geometrical technique is built on a significant amount of challenging outcomes and the correlation relating to the material array order, the light spectrum, as well as wave transport constituents. In metamaterials, improved conduction resonance by sub-wavelength apertures of quasi-crystal arrays was demonstrated in (Matsui et al., 2007), in addition to the transmission of broadband at terahertz radiation using improved efficiency by means of quasi-periodic grating assemblies (Ren et al., 2015).

Furthermore, aperiodic arrays of silver nano-wires exhibiting solid magnetic resonance at the optical frequency with negative active index have been studied recently (Agrawal et al., 2012). However, to extremely reduce the inbuilt optical losses of metamaterials, it has become highly necessary to implement next-generation devices with all-dielectric metastructures within a cost-effective and scalable fabrication technique. Recently, ultra-thin profile effective tunable metasurfaces (Liu et al., 2012) was proposed, using thermal effects (Dicken et al., 2009; Ou et al., 2011), electromechanical effects as a result of electrostatic forces (Ou et al., 2013), liquid crystals (Decker et al., 2013), and mechanical deformation (Pryce et al., 2011). They also show excellent potentials for studying biological and chemical challenges. Similarly, bio-sensing devices enabled by metamaterials could attain mono-layer (Wu et al., 2012; Yanik et al., 2011), picogram (Hendry et al., 2010), as well as reaching single-molecular (Kravets et al., 2013) sensitivity.

The main challenge facing the community of optical metamaterial is the constituent dielectric, which is required to have a refractive index comparable to the air interface. As revealed by the authors in (Ginn et al., 2012), any indices lower than $n{\sim}3.5$ will create large dispersion. Even though this must not be regarded as a tough limit, since it depends solely on the filling fraction and the resonator shape, it offers an excellent rule of thumb.

Since the main constituent dielectric is usually a semiconductor material, effectively controlling the material optical characteristics will be interesting research. Nevertheless, it has proved difficult to attain to date. A similar area of research is the advancement of nonlinear optical metamaterials in which the nonlinear resonator surface susceptibility is improved with the cell unit geometry (Shcherbakov et al., 2014). The implementation of colloidal NPs, particularly Silicon spheres, is an attractive method that is presently undergoing development. Nevertheless, procedures are also required that permit added controllability in guiding the cell unit geometry.

6. Conclusions

In this article, we have presented the recent state-of-the-art review in the field of optical metamaterials from a fresh and fundamental principle. We described the appropriate material structures that enable us to specify the effective electromagnetic properties in the visible light region. The most recent 2D theoretical modeling of optical metasurfaces is discussed. On this basis, we revisited a general electromagnetic homogenization theory that considers available models to other general conditions. We also discussed the recent advances in theoretical modeling and nanofabrication methods that could enable the realization of 3D optical metamaterials. We reflected on a number of the recent progress that sparks new light in optical metamaterial research. Nevertheless, several challenges still need to be resolved, such as intrinsic metal material losses and developing highly precise simulation software able to deal with the complexity of devices. Novel research directions are emerging for optical metamaterials, including random access 2D and 3D optical metamaterials, dynamic 3D holographic displays, cognitive metasystems, reconfigurable photonic circuits, reconfigurable large area metasurfaces for dynamic paint, and high feature resonance ($Q > 10\,000$) sensing. Nevertheless, the fabrication of high-throughput photonic metamaterials still remains a major setback, thus there are promising prospects in molecular manufacturing by means of kinematic self-replicating machines, DNA scaffolding, and diamond mechanosynthesis.

Acknowledgement

This research did not receive any specific grant from funding agencies in the public, commercial, or non-profit sectors. However, the authors wish to thank the Department of Communication Engineering, Ahmadu Bello University, Zaria, Nigeria for providing an excellent research environment to complete this work.

References

Agrawal, A., Park, W. & Piestun, R. (2012) Negative permeability with arrays of aperiodic silver nanoclusters. Applied Physics Letters, 101**,** 083109.

Al-Joumayly, M.A. and Behdad, N. (2011) Wideband planar microwave lenses using sub-wavelength spatial phase shifters. IEEE Transactions on Antennas and Propagation, 59**:** 4542-4552.

Albertoni, A. (2011) Long wave infrared metamaterials and nano-materials design, simulation, and laboratory test for target camouflage in the defence application. Electro-Optical and Infrared Systems: Technology and Applications VIII, 2011. International Society for Optics and Photonics, 818509.

Albooyeh, M., Morits, D. and Simovski, C. (2011) Electromagnetic characterization of substrated metasurfaces. Metamaterials, 5**:** 178-205.

Andersson, K.E. and Åkerlind, C. (2014) A review of materials for spectral design coatings in signature management applications. Optics and Photonics for Counterterrorism, Crime Fighting, and Defence X; and Optical Materials and Biomaterials in Security and Defence Systems Technology XI, 2014. International Society for Optics and Photonics, 92530Y.

Bansal, R. (2011) Bending Snell's Laws [AP-S Turnstile]. IEEE Antennas and Propagation Magazine, 53**:** 146-147.

Belov, P.A. and Simovski, C.R. (2005). Homogenization of electromagnetic crystals formed by uniaxial resonant scatterers. Physical Review E, 72, 026615.

Beruete, M., Sorolla, M., Marqués, R., Baena, J. and Freire, M. (2006) Resonance and cross-polarization effects in conventional and complementary split ring resonator periodic screens. Electromagnetics, 26**:** 247-260.

Boltasseva, A. and Shalaev, V.M. (2008) Fabrication of optical negative-index metamaterials: Recent advances and outlook. Metamaterials, 2**:** 1-17.

Brizzi, A., Pellegrini, A. and Hao, Y. (2012) Design of a cylindrical resonant cavity antenna for BAN applications at V band. Antenna Technology (iWAT), 2012 IEEE International Workshop on, 2012. IEEE, 152-155.

Buonsanti, R. and Milliron, D.J. (2013) Chemistry of doped colloidal nanocrystals. Chemistry of Materials, 25**:** 1305-1317.

Cai, W., Chettiar, U.K., Kildishev, A.V. and Shalaev, V.M. (2007) Optical cloaking with metamaterials. Nature photonics, 1**,** 224.

Chaurasiya, D., Ghosh, S. and Srivastava, K.V. (2014) Dual band polarization-insensitive wide angle metamaterial absorber for radar application. Microwave Conference (EuMC), 2014 44th European, 2014. IEEE, 885-888.

Chen, H.T., Taylor, A.J. and Yu, N. (2016) A review of metasurfaces: physics and applications. Reports on Progress in Physics, 79**,** 076401.

Chen, W., Tymchenko, M., Gopalan, P., Ye, X., Wu, Y., Zhang, M., Murray, C.B., Alu, A. and Kagan, C.R. (2015) Large-area nanoimprinted colloidal Au nanocrystal-based nanoantennas for ultrathin polarizing plasmonic metasurfaces. Nano letters, 15: 5254-5260.

Chon, J.W. and Iniewski, K. (2013) Nanoplasmonics: advanced device applications, CRC Press.

Cui, T.J., Qi, M.Q., Wan, X., Zhao, J. and Cheng, Q. (2014) Coding metamaterials, digital metamaterials and programmable metamaterials. Light: Science & Applications, 3**,** e218.

Decker, M., Klein, M., Wegener, M. and Linden, S. (2007) Circular dichroism of planar chiral magnetic metamaterials. Optics letters, 32**:** 856-858.

Decker, M., Kremers, C., Minovich, A., Staude, I., Miroshnichenko, A.E., Chigrin, D., Neshev, D.N., Jagadish, C. and Kivshar, Y.S. (2013) Electro-optical switching by liquid-crystal controlled metasurfaces. Optics express, 21**:** 8879-8885.

Dicken, M.J., Aydin, K., Pryce, I.M., Sweatlock, L.A., Boyd, E.M., Walavalkar, S., Ma, J. and Atwater, H.A. (2009) Frequency tunable near-infrared metamaterials based on VO 2 phase transition. Optics express, 17**:** 18330-18339.

Dimitriadis, A.I., Kantartzis, N.V., Rekanos, I.T. and Tsiboukis, T.D. (2012) Efficient metafilm/metasurface characterization for obliquely incident TE waves via surface susceptibility models. IEEE Transactions on Magnetics, 48**:** 367-370.

Dimitriadis, A.I., Sounas, D.L., Kantartzis, N.V., Caloz, C. and Tsiboukis, T.D. (2012) Surface susceptibility bianisotropic matrix model for periodic metasurfaces of uniaxially mono-anisotropic scatterers under oblique TE-wave incidence. IEEE Transactions on Antennas and Propagation, 60: 5753-5767.

Dolling, G., Enkrich, C., Wegener, M., Zhou, J., Soukoulis, C.M. and Linden, S. (2005) Cut-wire pairs and plate pairs as magnetic atoms for optical metamaterials. Optics letters, 30**:** 3198-3200.

Dong, Y. and Liu, S. (2012) Topology optimization of patch-typed left-handed metamaterial configurations for transmission performance within the radio frequency band based on the genetic algorithm. Journal of Optics, 14**,** 105101.

Estakhri, N.M.and Alù, A. (2016) Recent progress in gradient metasurfaces. JOSA B, 33**,** A21-A30.

Fafarman, A.T., Hong, S.H., Caglayan, H., Ye, X., Diroll, B.T., Paik, T., Engheta, N., Murray, C.B. and Kagan, C.R. (2012) Chemically tailored dielectric-to-metal transition for the design of

metamaterials from nanoimprinted colloidal nanocrystals. Nano letters, 13**:** 350-357.

Fan, J.A., Bao, K., Sun, L., Bao, J., Manoharan, V.N., Nordlander, P. and Capasso, F. (2012) Plasmonic mode engineering with templated self-assembled nanoclusters. Nano letters, 12**:** 5318-5324.

Fleury, R. and Alu, A. (2014) Cloaking and invisibility: A review. Forum for Electromagnetic Research Methods and Application Technologies, 1:9.

Fontana, J. and Ratna, B.R. (2015) Toward high throughput optical metamaterial assemblies. Applied optics, 54**:** F61-F69.

Forestiere, C., Pasquale, A.J., Capretti, A., Miano, G., Tamburrino, A., Lee, S.Y., Reinhard, B.R.M. and Dal Negro, L. (2012) Genetically engineered plasmonic nanoarrays. Nano letters, 12**:** 2037-2044.

Fruhnert, M., Mühlig, S., Lederer, F. and Rockstuhl, C. (2014) Towards negative index self-assembled metamaterials. Physical Review B, 89**,** 075408.

Garg, R., Bahl, I. and Bozzi, M. (2013) Microstrip lines and slotlines, Artech house.

Genevet, P. and Capasso, F. (2015) Holographic optical metasurfaces: a review of current progress. Reports on Progress in Physics, 78**,** 024401.

Ginn, J.C., Brener, I., Peters, D.W., Wendt, J.R., Stevens, J.O., Hines, P.F., Basilio, L.I., Warne, L.K., Ihlefeld, J.F. and Clem, P.G. (2012) Realizing optical magnetism from dielectric metamaterials. Physical review letters, 108**,** 097402.

Glybovski, S.B., Tretyakov, S.A., Belov, P.A., Kivshar, Y.S. and Simovski, C.R. (2016) Metasurfaces: From microwaves to visible. Physics Reports, 634**:** 1-72.

HäGglund, C., Zeltzer, G., Ruiz, R., Thomann, I., Lee, H.B.R., Brongersma, M.L. and Bent, S.F. (2013). Self-assembly based plasmonic arrays tuned by atomic layer deposition for extreme visible light absorption. Nano letters, 13**:** 3352-3357.

Hanuka, A., Goldemberg, E., Zilka, A. and Schächter, L. (2017) Artificial materials for structure-based laser acceleration. AIP Conference Proceedings, 2017. AIP Publishing, 060008.

Hanuka, A., Goldemberg, E., Zilka, A. and Schächter, L. (2018) Metamaterials for optical Bragg accelerators. Applied Physics Letters, 112**,** 101902.

Hendry, E., Carpy, T., Johnston, J., Popland, M., Mikhaylovskiy, R., Lapthorn, A., Kelly, S., Barron, L., Gadegaard, N. and Kadodwala, M. (2010) Ultrasensitive detection and characterization of biomolecules using superchiral fields. Nature nanotechnology, 5**,** 783.

Henzie, J., Lee, M.H. and Odom, T.W. (2007) Multiscale patterning of plasmonic metamaterials. Nature nanotechnology, 2**,** 549.

Holloway, C.L., Dienstfrey, A., Kuester, E.F., O'hara, J.F., Azad, A.K. and Taylor, A.J. (2009) A discussion on the interpretation and characterization of metafilms/metasurfaces: The two-dimensional equivalent of metamaterials. Metamaterials, 3**:** 100-112.

Holloway, C.L., Kuester, E.F. and Dienstfrey, A. (2011) Characterizing metasurfaces/metafilms: The connection between surface susceptibilities and effective material properties. IEEE Antennas and Wireless Propagation Letters, 10**:** 1507-1511.

Holloway, C.L., Kuester, E.F., Gordon, J.A., O'hara, J., Booth, J. and Smith, D.R. (2012) An overview of the theory and applications of metasurfaces: The two-dimensional equivalents of metamaterials. IEEE Antennas and Propagation Magazine, 54**:** 10-35.

Holloway, C.L., Mohamed, M.A., Kuester, E.F. and Dienstfrey, A. (2005) Reflection and transmission properties of a metafilm: With an application to a controllable surface composed of resonant particles. IEEE Transactions on Electromagnetic Compatibility, 47**:** 853-865.

Hsiao, H.H., Chu, C.H. and Tsai, D.P. (2017) Fundamentals and applications of metasurfaces. Small Methods.

Hsiao, H.H., Chu, C.H. and Tsai, D.P. (2017) Fundamentals and applications of metasurfaces. Small Methods, 1**,** 1600064.

Idemen, M. (1988) Straightforward derivation of boundary conditions on sheet simulating an anisotropic thin layer. Electronics Letters, 24**:** 663-665.

Ishikawa, A. and Tanaka, T. (2006) Negative magnetic permeability of split ring resonators in the visible light region. Optics communications, 258**:** 300-305.

Ishikawa, A., Tanaka, T. and Kawata, S. (2005) Negative magnetic permeability in the visible light region. Physical review letters, 95**:** 237401.

Ishikawa, A., Tanaka, T. and Kawata, S. (2007) Frequency dependence of the magnetic response of split-ring resonators. JOSA B, 24**:** 510-515.

Iwanaga, M. (2012) Photonic metamaterials: a new class of materials for manipulating light waves. Science and technology of advanced materials, 13**,** 053002.

Jakšić, Z. (2010) Optical metamaterials as the platform for a novel generation of ultrasensitive chemical or biological sensors. Metamaterials: Classes, Properties and Applications**,** 1-42.

Johnson, P.B. and Christy, R.W. (1972) Optical constants of the noble metals. Physical review B, 6**,** 4370.

Jones, A., Nye, J. and Greenberg, A. (2013) Nanotechnology in the Military. Nanoscale Science and Engineering Center, The University of Wisconsin, Madison.

Kelkar, A. (1991) Flaps: conformal phased reflecting surfaces. Radar Conference, 1991. Proceedings of IEEE National, 1991. IEEE, 58-62.

Khorasaninejad, M., Chen, W.T., Zhu, A.Y., Oh, J., Devlin, R.C., Roques-Carmes, C., Mishra, I. and Capasso, F. (2017) Visible wavelength planar metalenses based on titanium dioxide. IEEE Journal of Selected Topics in Quantum Electronics, 23: 43-58.

Khurgin, J.B. (2015) How to deal with the loss in plasmonics and metamaterials. Nature nanotechnology, 10**,** 2.

Kildishev, A.V., Boltasseva, A. and Shalaev, V.M. (2013) Planar photonics with metasurfaces. Science, 339**,** 1232009.

Kravets, V., Schedin, F., Jalil, R., Britnell, L., Gorbachev, R., Ansell, D., Thackray, B., Novoselov, K., Geim, A. and Kabashin, A.V. (2013) Singular phase nano-optics in plasmonic metamaterials for label-free single-molecule detection. Nature materials, 12**,** 304.

Kuester, E.F., Mohamed, M.A., Piket-May, M. and Holloway, C.L. (2003) Averaged transition conditions for electromagnetic fields at a metafilm. IEEE Transactions on Antennas and Propagation, 51**:** 2641-2651.

Kumar, A., Abegaonkar, M.P. and Koul, S.K. (2016) Triple band miniaturized patch antenna loaded with metamaterial unit cell for defense applications. Industrial and Information Systems (ICIIS), 2016 11th International Conference on, 2016. IEEE, 833-837.

Lalanne, P. and Chavel, P. (2017) Metalenses at visible wavelengths: past, present, perspectives. Laser & Photonics Reviews, 11**,** 1600295.

Lapine, M., Shadrivov, I.V. and Kivshar, Y.S. (2014) Colloquium: nonlinear metamaterials. Reviews of Modern Physics, 86**,** 1093.

Larouche, S. and Smith, D.R. (2012) Reconciliation of generalized refraction with diffraction theory. Optics letters, 37**:** 2391-2393.

Lheurette, É. (2013) Overview of Microwave and Optical Metamaterial Technologies. Metamaterials and Wave Control**,** 1-42.

Linden, S., Enkrich, C., Wegener, M., Zhou, J., Koschny, T. and Soukoulis, C.M. (2004) Magnetic response of metamaterials at 100 terahertz. Science, 306**:** 1351-1353.

Lindquist, N.C., Nagpal, P., Mcpeak, K.M., Norris, D.J. and Oh, S.H. (2012) Engineering metallic nanostructures for plasmonics and nanophotonics. Reports on Progress in Physics, 75**,** 036501.

Liu, A., Zhu, W., Tsai, D. and Zheludev, N.I. (2012) Micromachined tunable metamaterials: a review. Journal of Optics, 14**,** 114009.

Lohse, S.E. and Murphy, C.J. (2013) The quest for shape control: a history of gold nanorod synthesis. Chemistry of Materials, 25**:** 1250-1261.

Maier, S.A. and Atwater, H.A. (2005) Plasmonics: Localization and guiding of electromagnetic energy in metal/dielectric structures. Journal of applied physics, 98**,** 10.

Maier, S.A., Brongersma, M.L., Kik, P.G., Meltzer, S., Requicha, A.A. and Atwater, H.A. (2001) Plasmonics—a route to nanoscale optical devices. Advanced materials, 13**:** 1501-1505.

Matsui, T., Agrawal, A., Nahata, A. and Vardeny, Z.V. (2007) Transmission resonances through aperiodic arrays of subwavelength apertures. Nature, 446**,** 517.

Mcgrath, D. (1986) Planar three-dimensional constrained lenses. IEEE Transactions on Antennas and Propagation, 34**:** 46-50.

Meinzer, N., Barnes, W.L. and Hooper, I.R. (2014) Plasmonic meta-atoms and metasurfaces. Nature Photonics, 8**,** 889.

Minovich, A.E., Miroshnichenko, A.E., Bykov, A.Y., Murzina, T.V., Neshev, D.N. and Kivshar, Y.S. (2015) Functional and nonlinear optical metasurfaces. Laser & Photonics Reviews, 9**:** 195-213.

Mittra, R., Chan, C.H. and Cwik, T. (1988) Techniques for analyzing frequency selective surfaces-a review. Proceedings of the IEEE, 76**:** 1593-1615.

Morits, D. and Simovski, C. (2010) Electromagnetic characterization of planar and bulk metamaterials: A theoretical study. Physical Review B, 82**,** 165114.

Mousavi, S.H., Khanikaev, A.B. and Shvets, G. (2012) Optical properties of Fano-resonant metallic metasurfaces on a substrate. Physical Review B, 85**,** 155429.

Naik, G.V., Shalaev, V.M. and Boltasseva, A. (2013) Alternative plasmonic materials: beyond gold and silver. Advanced Materials, 25**:** 3264-3294.

Ou, J.Y., Plum, E., Jiang, L. and Zheludev, N.I. (2011) Reconfigurable photonic metamaterials. Nano letters, 11: 2142-2144.

Ou, J.Y., Plum, E., Zhang, J. and Zheludev, N.I. (2013) An electromechanically reconfigurable plasmonic metamaterial operating in the near-infrared. Nature nanotechnology, 8**,** nnano. 2013.25.

Ozbay, E. (2006) Plasmonics: merging photonics and electronics at nanoscale dimensions. science, 311: 189-193.

Pendry, J.B. (2014) Controlling light on the nanoscale (invited review). Progress In Electromagnetics Research, 147**:** 117-126.

Pendry, J.B., Holden, A.J., Robbins, D.J. and Stewart, W. (1999) Magnetism from conductors and enhanced nonlinear phenomena. IEEE transactions on microwave theory and techniques, 47**:** 2075-2084.

Pozar, D. (1996) Flat lens antenna concept using aperture coupled microstrip patches. Electronics Letters, 32: 2109-2111.

Pozar, D. and Metzler, T. (1993) Analysis of a reflectarray antenna using microstrip patches of variable size. Electronics Letters, 29**:** 657-658.

Pozar, D.M. (2011) Microwave Engineering. John Wiley and Sons.

Pozar, D.M., Targonski, S.D. and Syrigos, H. (1997) Design of millimeter wave microstrip reflectarrays. IEEE transactions on antennas and propagation, 45**:** 287-296.

Pryce, I.M., Aydin, K., Kelaita, Y.A., Briggs, R.M. and Atwater, H.A. (2011) Characterization of the tunable response of highly strained compliant optical metamaterials. Philosophical Transactions of the Royal Society of London A: Mathematical, Physical and Engineering Sciences, 369**:** 3447-3455.

Ren, X.P., Fan, R.H., Peng, R.W., Huang, X.R., Xu, D.H., Zhou, Y. and Wang, M. (2015) Nonperiodic metallic gratings transparent for broadband terahertz waves. Physical Review B, 91**,** 045111.

Rho, J. (2017) Realization of 3D Metamaterial and Plasmonic Devices at Optical Frequencies. Frontiers in Optics, 2017. Optical Society of America, FTh2D. 1.

Ross, M.B., Blaber, M.G. and Schatz, G.C. (2014) Using nanoscale and mesoscale anisotropy to engineer the optical response of three-dimensional plasmonic metamaterials. Nature Communications, 5**,** 4090.

Ross, M.B., Ku, J.C., Vaccarezza, V.M., Schatz, G.C. and Mirkin, C.A. (2015) Nanoscale form dictates mesoscale function in plasmonic DNA–nanoparticle superlattices. Nature nanotechnology, 10**,** 453.

Rycenga, M., Cobley, C.M., Zeng, J., Li, W., Moran, C.H., Zhang, Q., Qin, D. and Xia, Y. (2011) Controlling the synthesis and assembly of silver nanostructures for plasmonic applications. Chemical reviews, 111**:** 3669-3712.

Schuller, J.A., Barnard, E.S., Cai, W., Jun, Y.C., White, J.S. and Brongersma, M.L. (2010) Plasmonics for extreme light concentration and manipulation. Nature materials, 9**,** 193.

Shalaev, V.M., Cai, W., Chettiar, U.K., Yuan, H.K., Sarychev, A.K., Drachev, V.P. & Kildishev, A.V. (2005) Negative index of refraction in optical metamaterials. Optics letters, 30**:** 3356-3358.

Shaltout, A.M., Kildishev, A.V. and Shalaev, V.M. (2016). Evolution of photonic metasurfaces: from static to dynamic. JOSA B, 33**:** 501-510.

Shcherbakov, M.R., Neshev, D.N., Hopkins, B., Shorokhov, A.S., Staude, I., Melik-Gaykazyan, E.V., Decker, M., Ezhov, A.A., Miroshnichenko, A.E. and Brener, I. (2014) Enhanced third-harmonic generation in silicon nanoparticles driven by magnetic response. Nano letters, 14**:** 6488-6492.

Shelby, R.A., Smith, D.R. and Schultz, S. (2001) Experimental verification of a negative index of refraction. science, 292**:** 77-79.

Shvets, G., Trendafilov, S., Pendry, J. and Sarychev, A. (2007) Guiding, focusing, and sensing on the subwavelength scale using metallic wire arrays. Physical review letters, 99**,** 053903.

Simovski, C.R. (2010) On electromagnetic characterization and homogenization of nanostructured metamaterials. Journal of Optics, 13**,** 013001.

Smith, D.R., Padilla, W.J., Vier, D., Nemat-Nasser, S.C. and Schultz, S. (2000) Composite medium with simultaneously negative permeability and permittivity. Physical review letters, 84**,** 4184.

Smith, D.R., Pendry, J.B. and Wiltshire, M.C. (2004) Metamaterials and negative refractive index. Science, 305**:** 788-792.

Soukoulis, C.M. and Wegener, M. (2011) Past achievements and future challenges in the development of three-dimensional photonic metamaterials. nature photonics, 5**,** 523.

Sounas, D. and Kantartzis, N. (2009) Systematic surface waves analysis at the interfaces of composite DNG/SNG media. Optics Express, 17**:** 8513-8524.

Su, V.C., Chu, C.H., Sun, G. and Tsai, D.P. (2018) Advances in optical metasurfaces: fabrication and applications. Optics express, 26**:** 13148-13182.

Turpin, J.P., Bossard, J.A., Morgan, K.L., Werner, D.H. and Werner, P.L. (2014) Reconfigurable and tunable metamaterials: a review of the theory and applications. International Journal of Antennas and Propagation, 2014:429837.

Urbas, A.M., Jacob, Z., Dal Negro, L., Engheta, N., Boardman, A., Egan, P., Khanikaev, A.B., Menon, V., Ferrera, M. and Kinsey, N. (2016) Roadmap on optical metamaterials. Journal of Optics, 18**,** 093005.

Veselago, V.G. (1968) The electrodynamics of substances with simultaneously negative values of and μ. Soviet physics uspekhi, 10**,** 509.

Vignolini, S., Yufa, N.A., Cunha, P.S., Guldin, S., Rushkin, I., Stefik, M., Hur, K., Wiesner, U., Baumberg, J.J. and Steiner, U. (2012) A 3D optical metamaterial made by self-assembly. Advanced Materials, 24: 23-27.

Walia, S., Shah, C.M., Gutruf, P., Nili, H., Chowdhury, D.R., Withayachumnankul, W., Bhaskaran, M. and Sriram, S. (2015) Flexible metasurfaces and metamaterials: a review of materials and fabrication processes at micro-and nano-scales. Applied Physics Reviews, 2**,** 011303.

West, P.R., Ishii, S., Naik, G.V., Emani, N.K., Shalaev, V.M. and Boltasseva, A. (2010) Searching for better plasmonic materials. Laser & Photonics Reviews, 4**:** 795-808.

Wu, C., Khanikaev, A.B., Adato, R., Arju, N., Yanik, A.A., Altug, H. and Shvets, G. (2012) Fano-resonant asymmetric metamaterials for ultrasensitive spectroscopy and identification of molecular monolayers. Nature materials, 11**,** 69.

Wu, M.C.T. (2018) Ultrafast Target Detection Based On Microwave Metamaterials. US Patent App. 15/553,921.

Yanik, A.A., Cetin, A.E., Huang, M., Artar, A., Mousavi, S.H., Khanikaev, A., Connor, J.H., Shvets, G. and Altug, H. (2011) Seeing protein monolayers with naked eye through plasmonic Fano resonances. Proceedings of the National Academy of Sciences, 108**:** 11784-11789.

Ye, X., Chen, J., Diroll, B.T. and Murray, C.B. (2013) Tunable plasmonic coupling in self-assembled binary nanocrystal superlattices studied by correlated optical microspectrophotometry and electron microscopy. Nano letters, 13**:** 1291-1297.

Ye, X., Fei, J., Diroll, B.T., Paik, T. and Murray, C.B. (2014) Expanding the spectral tunability of plasmonic resonances in doped metal-oxide nanocrystals through cooperative cation–anion codoping. Journal of the American Chemical Society, 136**:** 11680-11686.

Ye, X., Zheng, C., Chen, J., Gao, Y. and Murray, C.B. (2013) Using binary surfactant mixtures to simultaneously improve the dimensional tunability and monodispersity in the seeded growth of gold nanorods. Nano letters, 13**:** 765-771.

Yoon, G., Kim, I. and Rho, J. (2016) Challenges in fabrication towards realization of practical metamaterials. Microelectronic Engineering, 163**:** 7-20.

Yu, N. and Capasso, F. (2014) Flat optics with designer metasurfaces. Nature materials, 13**,** 139.

Yu, N., Genevet, P., Kats, M.A., Aieta, F., Tetienne, J.P., Capasso, F. and Gaburro, Z. (2011) Light propagation with phase discontinuities: generalized laws of reflection and refraction. science, 334: 333-337.

Zaghloul, A.I., Weiss, S.J. and Coburn, W.K. (2010) Antenna Developments for Military Applications. ACES.

Zhang, L., Mei, S., Huang, K. and Qiu, C.W. (2016) Advances in full control of electromagnetic waves with metasurfaces. Advanced Optical Materials, 4**:** 818-833.

Zhao, Y., Liu, X.X. and Alù, A. (2014) Recent advances on optical metasurfaces. Journal of Optics, 16**,** 123001.

Zheludev, N.I. and Kivshar, Y.S. (2012) From metamaterials to metadevices. Nature materials, 11**,** 917.

Zhu, A.Y., Kuznetsov, A.I., Luk'yanchuk, B., Engheta, N. and Genevet, P. (2017) Traditional and emerging materials for optical metasurfaces. Nanophotonics, 6**:** 452-471.